Ain Shams Engineering Journal (2016) 7, 249–264

Ain Shams University

Ain Shams Engineering Journal

www.elsevier.com/locate/asej
www.sciencedirect.com

ELECTRICAL ENGINEERING

Impact of DC link control strategies on the power-flow convergence of integrated AC–DC systems

Shagufta Khan *, **Suman Bhowmick** [1]

Department of Electrical Engineering, Delhi Technological University, Delhi 110042, India

Received 22 November 2014; revised 3 March 2015; accepted 14 April 2015
Available online 19 May 2015

KEYWORDS

AC–DC power-flow;
Newton Raphson method;
HVDC control strategy

Abstract For the power-flow solution of integrated AC–DC systems, five quantities are required to be solved per converter, against three independent equations available. These three equations consist of two basic converter equations and one DC network equation, corresponding to each converter. Thus, for solution, two additional equations are required. These two equations are derived from the control specifications adopted for the DC link. Depending on the application, several combinations of valid control specifications are possible. A set of valid control specifications constitutes a control strategy. It is observed that the control strategy adopted for the DC link strongly affects the power-flow convergence of integrated AC–DC systems. This paper investigates how different control strategies affect the power flow convergence of integrated AC–DC systems. Sequential method is used to solve the DC variables in the Newton Raphson (NR) power flow model. Seven typical control strategies have been taken into consideration. This is validated by numerous case studies carried out with multiple DC links incorporated in the IEEE 118-bus and 300-bus test systems.

1. Introduction

With ever-increasing load demands, system stability issues and different operating frequencies may render AC transmission infeasible. In this respect, HVDC transmission allows power transmission between asynchronous AC transmission systems, and can increase the system stability by preventing cascading failures due to phase instability from propagating from one part of a wider power transmission grid to another. For lengths exceeding about 500 km, HVDC transmission is proving to be more economical than AC [1–3].

For planning, operation and control of power systems with HVDC links, power-flow solution of power systems incorporated with HVDC links is required [4–6]. For power flow solution of hybrid AC–DC systems, corresponding to each converter, five quantities are required to be solved. These are the DC voltage, the DC current, the control angle, the converter transformer tap ratio and the converter power factor.

* Corresponding author. Mobile: +91 9015676753.
E-mail addresses: khan.shagufta7@gmail.com (S. Khan), suman.bhowmick@dce.ac.in (S. Bhowmick).
[1] Mobile: +91 9968499840.

Peer review under responsibility of Ain Shams University.

ELSEVIER Production and hosting by Elsevier

http://dx.doi.org/10.1016/j.asej.2015.04.004
2090-4479 © 2015 Faculty of Engineering, Ain Shams University. Production and hosting by Elsevier B.V.

List of symbols

S_{base} base MVA
$V_{ac\ base}, I_{ac\ base}, Z_{ac\ base}$ AC base voltage, AC base current and AC base impedance, respectively
$V_{dc\ base}, I_{dc\ base}, Z_{dc\ base}$ DC base voltage, DC base current and DC base impedance, respectively
n_b number of bridges
X_c commutating reactance
V_d, I_d DC voltage and current, respectively
ϕ_R, ϕ_I power factor angles at the rectifier and inverter ends, respectively
α_R, γ_I firing angle of the rectifier and extinction angle of the inverter, respectively
V_{dR}, V_{dI} DC voltages at the rectifier and inverter sides, respectively
a_R, a_I converter transformer tap ratios on the rectifier and inverter sides, respectively
R_d resistance of DC link
$V_i\angle\theta_i$ AC bus voltage magnitude (rms) and phase angle at ith bus
$V_j\angle\theta_j$ AC bus voltage magnitude (rms) and phase angle at jth bus
Y_{ik}, ϕ_{ik} magnitude and phase angle of the element in the ith row and kth column of the bus admittance matrix
P_{Di}, Q_{Di} active and reactive power demands at bus 'i', respectively
P_{Dj}, Q_{Dj} active and reactive power demands at bus 'j', respectively
V_{doR}, V_{doI} no load direct voltages at the rectifier and inverter sides, respectively
P_{dR}, Q_{dR} active and reactive powers at the rectifier side, respectively
P_{dI}, Q_{dI} active and reactive powers at the inverter side, respectively

On the other hand, only three independent equations comprising two basic converter equations and one DC network equation exist per converter. Thus for solution, two additional equations are required. These two equations are obtained from the control specifications adopted for the DC link. Thus, mathematically, the control specifications are used to bridge the gap between the number of independent equations and the number of unknowns. Control specifications usually include specified values of converter transformer tap ratio, converter control angle, DC voltage, DC current or power. Several combinations of valid control specifications are feasible, depending on the application. Each set of valid control specifications is known as a control strategy. Although a large number of control strategies are feasible, only some are adopted in practice.

The earliest algorithms for power flow were based on the Gauss–Siedel method, which exhibited poor convergence characteristics. Subsequently, the Newton–Raphson (NR) method was developed, which had better convergence characteristics. Gradually, it was adopted as the de facto standard in the industry.

For power flow solution of integrated AC–DC systems using the NR method, two different algorithms have generally been reported in the literature. These are known as the unified and the sequential method, respectively. Some excellent research works on the unified and the sequential power flow methods are presented in [4–15], respectively. Unlike the unified method, the sequential method is easier to implement and poses lesser computational burden due to the smaller size of the Jacobian matrix. Consequently, in this work, only the sequential AC–DC power-flow algorithm has been considered.

In the sequential AC–DC power-flow algorithm, the AC and DC systems are solved separately in each iteration and are coupled by injecting an equivalent amount of real and reactive power at the terminal AC buses. It is observed that each control strategy affects the sequential power flow convergence in a uniquely different manner. It was reported by [11] that for standard control strategies e.g. constant DC voltage or current or power, the convergence rate can be improved by decoupling the DC and AC systems and solving them independently. On the other hand, for non-standard ones such as constant tap ratios and constant terminal voltage, the convergence may suffer. The mechanism by which this occurs has not been very clear and has not been exclusively addressed in the literature. This motivated the authors to investigate how different control strategies affect the power flow convergence. Numerous case studies are carried out by adopting seven different control strategies on HVDC links incorporated in the IEEE 118-bus and 300-bus test systems [16] for validation.

This paper is organized as follows: In Section 2, the mathematical modeling of the integrated AC–DC system is presented. Section 3 details some of the typical DC link control strategies adopted in practice. In Section 4, the power flow equations of the integrated AC–DC system are presented, with the DC link acting as an equivalent load on the converter AC buses. Section 5 details the case studies carried out by incorporating DC links in the IEEE 118 and 300 bus test systems. The conclusions are presented in Section 6.

2. System modelling

Fig. 1 shows a typical AC–DC power system network in which a HVDC link is connected in the branch "i–j" between any two buses "i" and "j" of the network. The two converters representing the rectifier and the inverter are connected to the AC system at buses "i" and "j" respectively, through their respective converter transformers. The HVDC link is accounted for as equivalent amount of real and reactive power injections P_{dR} and Q_{dR}, P_{dI} and Q_{dI} at the converters' AC terminal buses "i" and "j", respectively. Although these power injections are not shown in Fig. 1, they are included in the analysis by appropriate modifications of the power flow equations, as detailed later in Section 4. Fig. 2 shows the equivalent circuit for the network shown in Fig. 1.

Prior to the selection of variables and formulation of the equations, several basic assumptions are required which are generally accepted in the analysis of steady state DC converter operation [1–3]. These are as follows:

- The AC voltages at the terminal bus bars are balanced and sinusoidal.

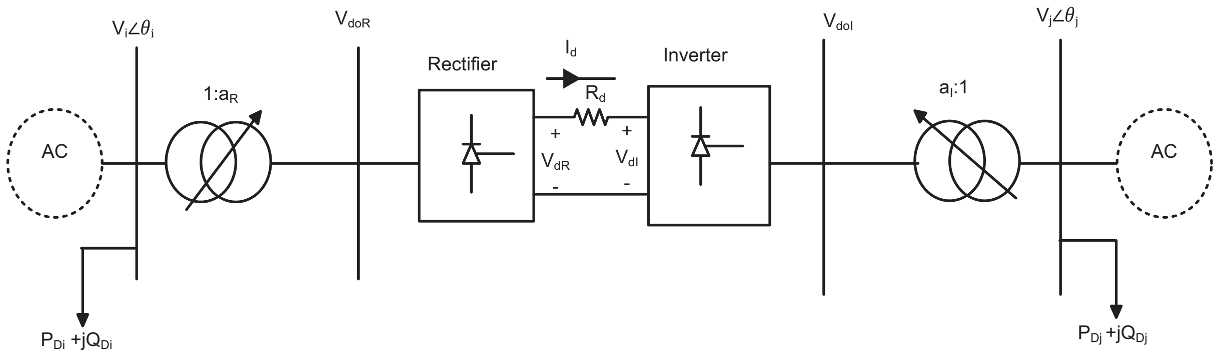

Figure 1 HVDC link between buses '*i*' and '*j*' of an existing power system network.

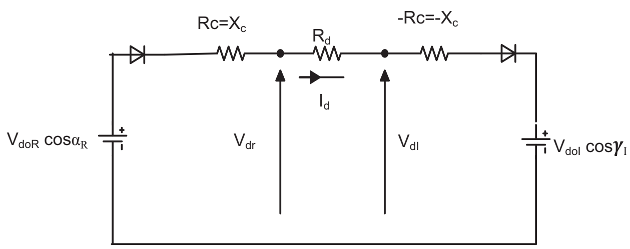

Figure 2 Equivalent circuit diagram for AC–DC interconnection.

- The converter operation is perfectly balanced.
- The direct current and voltage are smooth.
- The converter transformer is lossless and the magnetizing admittance is ignored.

Subsequently, for hybrid power flow calculations, the DC and AC equations are combined together. This necessitates the translation of the converter equations into the per-unit system as per the base values adopted in Appendix A, in order to use them with the AC system per-unit equations. These are shown in Table 1.

From Table 1, it can be observed that seven independent equations involving eleven unknowns are present. Hence, for a complete solution of the HVDC quantities, four variables (two per converter) are needed to be specified. These are derived from the control specifications adopted for the DC link. Several combinations of control specifications are possible and each combination comprises a control mode or strategy. This is elaborated in the next section.

Table 1 Basic HVDC equations in per unit.

$V_{dR} = a_R V_i cos\alpha_R - X_c I_d$	(1)
$V_{dI} = a_I V_j cos\gamma_I - X_c I_d$	(2)
$V_{dR} = a_R V_i cos\phi_R$	(3)
$V_{dI} = a_I V_j cos\phi_I$	(4)
$I_d = \frac{V_{dR} - V_{dI}}{R_d}$	(5)
$P_{dR} = V_{dR} I_d$	(6)
$P_{dI} = V_{dI} I_d$	(7)

Table 2 HVDC control strategies.

Control strategies	Specified quantities	Unknown quantities
1	$\alpha_R, P_{dR}, \gamma_I, V_{dI}$	$a_R, a_I, V_{dR}, \phi_R, \phi_I, I_d, P_{dI}$
2	a_R, P_{dR}, a_I, V_{dI}	$\alpha_R, \gamma_I, V_{dR}, \phi_R, \phi_I, I_d, P_{dI}$
3	$\alpha_R, I_d, \gamma_I, V_{dI}$	$a_R, a_I, V_{dR}, \phi_R, \phi_I, P_{dR}, P_{dI}$
4	$\alpha_R, P_{dR}, a_I, V_{dI}$	$a_R, \gamma_I, V_{dR}, \phi_R, \phi_I, I_d, P_{dI}$
5	$a_R, P_{dR}, \gamma_I, V_{dI}$	$\alpha_R, a_I, V_{dR}, \phi_R, \phi_I, P_{dI}, I_d$
6	$a_R, P_{dR}, \gamma_I, a_I$	$\alpha_R, V_{dR}, V_{dI}, \phi_R, \phi_I, I_d, P_{dI}$
7	$V_{dR}, I_d, a_I, \alpha_R$	$V_{dI}, \gamma_I, P_{dR}, a_R, \phi_R, \phi_I, P_{dI}$

3. HVDC control strategies

As already discussed in the last section, several control modes or strategies are possible corresponding to different combinations of the four control variables. Although many control strategies are feasible, however, due to a lack of space, only seven typical ones have been considered in this work. These are shown in Table 2, and are elaborated below.

3.1. Control strategy 1

In this control strategy, the firing angle of the rectifier and the extinction angle of the inverter are specified. The tap ratios of both the converter transformers 'a_R' and 'a_I' are calculated subsequent to the AC load flow.

3.2. Control strategy 2

In this strategy, the firing angle of the rectifier and extinction angle of the inverter are computed while their transformer tap ratios are specified. As the injected reactive power representing the converters gets updated every iteration, this control strategy is slightly harder to implement than the others.

3.3. Control strategy 3

This control strategy is also known as the constant current and voltage controlled mode. As in control strategy 1, both the converter transformer tap ratios 'a_R' and 'a_I' can be calculated subsequent to the AC load flow.

3.4. Control strategy 4

In this control strategy, the firing angle on the rectifier side is specified along with the tap ratio of the inverter

Table 3 First study of IEEE 118-bus system.

HVDC link		P_{base} (pu)	HVDC link specification		Power flow solution			
From bus no	To bus no		Spec. values		ACSV		DCSV	
			Control strategy 1		AC terminal buses		HVDC variables	
11	13	0.4081	P_{dR} (pu)	0.5	V_{11}	0.9803	V_{dR}	1.005
							I_d	0.4975
			V_{dI} (pu)	1.0	θ_{11}	10.739°	a_R	1.08
							a_I	1.15
			α_R (deg.)	5°	V_{13}	0.9598	$cos\phi_R$	0.94
							$cos\phi_I$	0.90
			γ_I (deg.)	18°	θ_{13}	11.349°	NI	6
			Control strategy 2		AC terminal buses		HVDC variables	
			P_{dR} (pu)	0.5	V_{11}	0.9801	V_{dR}	1.005
							I_d	0.4975
			V_{dI} (pu)	1	θ_{11}	10.741°	α_R	9.1566°
							γ_I	17.969°
			a_R	1.09	V_{13}	0.9596	$cos\phi_R$	0.94
							$cos\phi_I$	0.90
			a_I	1.15	θ_{13}	11.351°	NI	13
			Control strategy 3		AC terminal buses		HVDC variables	
			I_d (pu)	0.5	V_{11}	0.9803	V_{dR}	1.005
							P_{dR}	0.5025
			V_{dI} (pu)	1	θ_{11}	10.737°	a_R	1.08
							a_I	1.15
			α_R (deg.)	5°	V_{13}	0.9597	$cos\phi_R$	0.94
							$cos\phi_I$	0.90
			γ_I (deg.)	18°	θ_{13}	11.358°	NI	6
			Control strategy 4		AC terminal buses		HVDC variables	
			P_{dR} (pu)	0.5	V_{11}	0.9843	V_{dR}	1.005
							I_d	0.4975
			V_{dI} (pu)	1	θ_{11}	10.727°	a_R	1.08
							γ_I	17.868°
			α_R (deg.)	5	V_{13}	0.9767	$cos\phi_R$	0.94
							$cos\phi_I$	0.90
			a_I	1.13	θ_{13}	11.099°	NI	6
			Control strategy 5		AC terminal buses		HVDC variables	
			P_{dR} (pu)	0.5	V_{11}	0.9847	V_{dR}	1.005
							I_d	0.4975
			V_{dI} (pu)	1	θ_{11}	10.702°	α_R	10.678°
							a_I	1.13
			a_R	1.09	V_{13}	0.977	$cos\phi_R$	0.93
							$cos\phi_I$	0.90
			γ_I (deg.)	18°	θ_{13}	11.069°	NI	6
			Control strategy 6		AC terminal buses		HVDC variables	
			P_{dR} (pu)	0.5	V_{11}	0.9809	V_{dR}	0.9076
							I_d	0.5509
			a_R	1	θ_{11}	10.755°	V_{dI}	0.902
							α_R	10.707°
			a_I	1.05	V_{13}	0.9624	$cos\phi_R$	0.92
							$cos\phi_I$	0.89
			γ_I (deg.)	18°	θ_{13}	11.335°	NI	9
			Control strategy 7		AC terminal buses		HVDC variables	
			V_{dR} (pu)	1	V_{11}	0.9817	V_{dI}	0.9965
							γ_I	15.4291°
			I_d (p.u.)	0.35	θ_{11}	10.8211°	a_R	1.09
							P_{dR}	0.35
			a_I	1.11	V_{13}	0.964	$cos\phi_R$	0.9277
							$cos\phi_I$	0.9313
			α_R (deg.)	6°	θ_{13}	10.7882°	NI	11

side transformer. The tap ratio on the rectifier side transformer 'a_R' along with the inverter side extinction angle can be calculated subsequent to the AC load flow.

3.5. Control strategy 5

In this control strategy, the extinction angle of the inverter is specified along with the tap ratio of the rectifier side. On the other hand, the firing angle of the rectifier and the inverter side transformer tap ratio is computed subsequent to the AC load flow.

3.6. Control strategy 6

In this control strategy, the firing angle and the dc voltage of the rectifier side is computed given the tap ratios of the converter transformers along with the extinction angle of the inverter. The equivalent reactive power injections on both the rectifier and inverter sides are updated in each iteration, rendering this control strategy slightly harder to implement.

3.7. Control strategy 7

In this control strategy, the extinction angle of the inverter and DC voltage of the Inverter are computed while the transformer tap ratio at the inverter side and the DC voltage of the rectifier are specified. The equivalent reactive power injection of the inverter is updated in each iteration, rendering this control strategy slightly harder to implement.

4. AC–DC power-flow equations

As discussed in Section 2, the effect of the DC link is included in the power flow equations by injecting equivalent amount of real and reactive powers at the terminal AC buses connected to the converters. This results in appropriate modifications of the mismatch equations at the converter terminal AC buses, as given below.

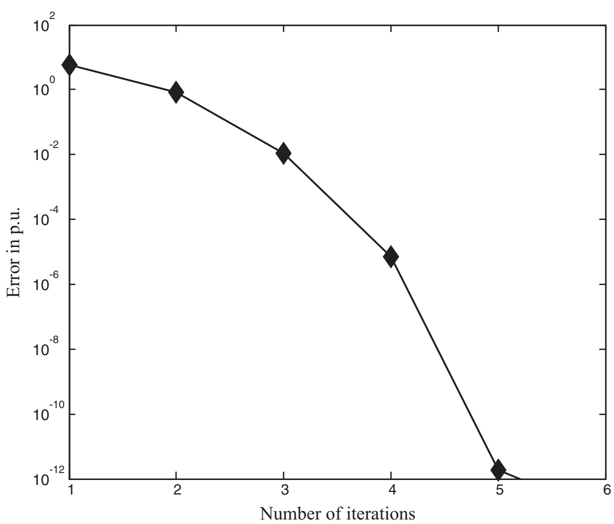

Figure 3 Convergence characteristics of base case power flow in IEEE-118 bus test system.

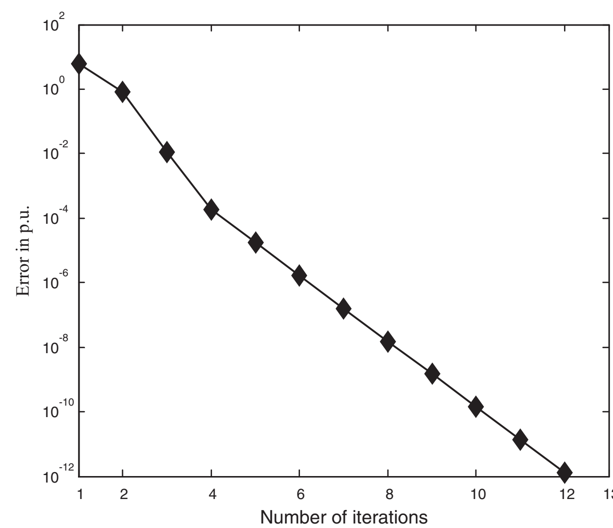

Figure 5 Convergence characteristics for the case study of Table 3 with control strategy 2.

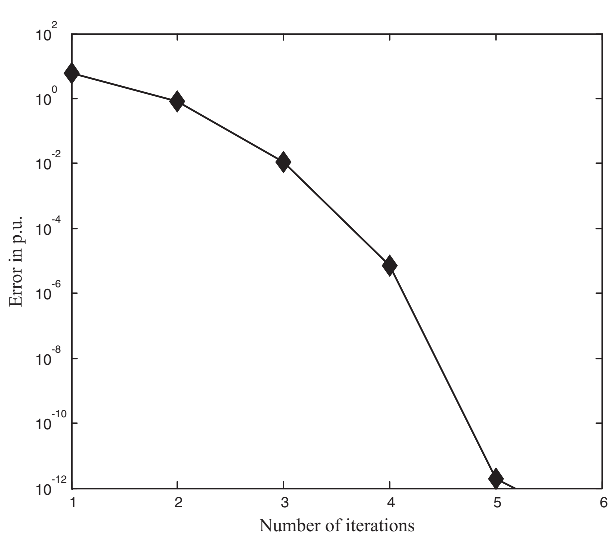

Figure 4 Convergence characteristics for the case study of Table 3 with control strategy 1.

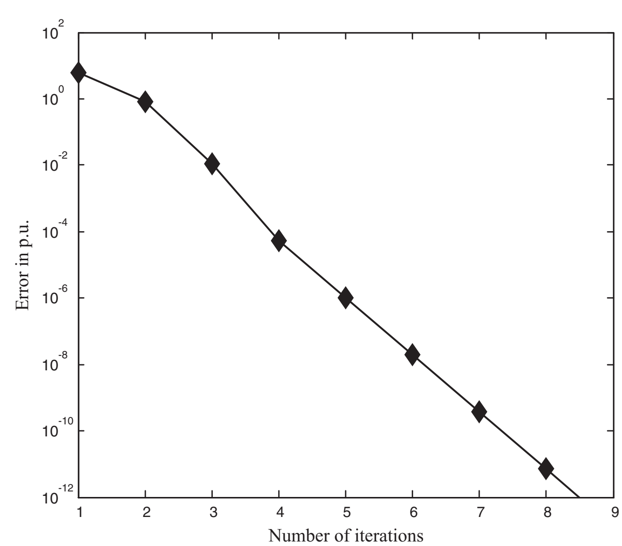

Figure 6 Convergence characteristics for the case study of Table 3 with control strategy 6.

For any AC bus 'i', which is not connected to any DC link, the mismatches in the active and reactive power injections are given respectively, by

$$\Delta P_i = P_i^{sp} - \sum_{k=1}^{n} V_i V_k Y_{ik} \cos(\theta_i - \theta_k - \phi_{ik}) \quad (8)$$

$$\Delta Q_i = Q_i^{sp} - \sum_{k=1}^{n} V_i V_k Y_{ik} \sin(\theta_i - \theta_k - \phi_{ik}) \quad (9)$$

If however, a DC link exists between arbitrary AC buses 'i' and 'j' with buses 'i' and 'j' connected to the rectifier and inverter respectively, the effect of the DC link can be incorporated in the AC power flow as equivalent active and reactive power injections 'P_{dR}' and 'Q_{dR}' at the rectifier bus 'i' and 'P_{dI}' and 'Q_{dI}' at the inverter bus 'j', respectively. Therefore, the mismatches in the active and reactive power injections can be written as

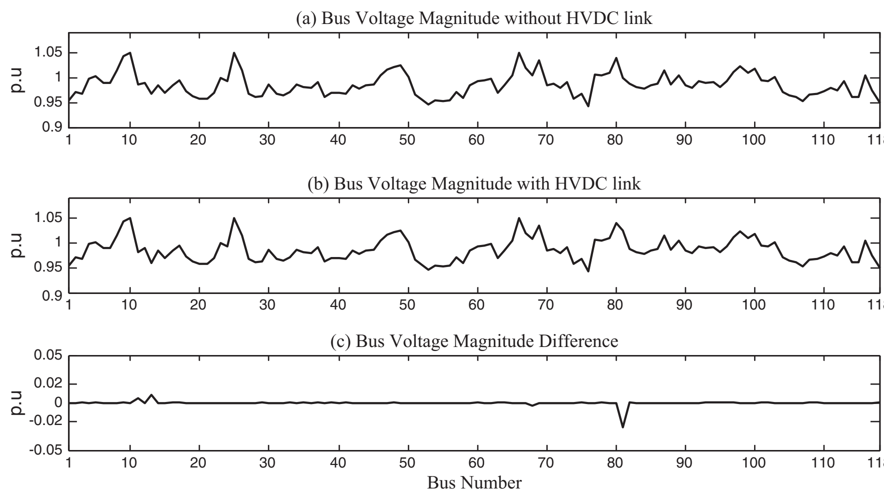

Figure 7 Bus voltage profile for the case study of Table 3 with control strategy 2.

Table 4 Variation of tap setting and reactive power consumption of rectifier with firing angle.

HVDC links		HVDC link specification	Power flow solutions		
Rectifier bus	Inverter bus	Control strategy-5	α_R (deg.)	AC terminal buses	HVDC variables
11	13	$\gamma_I = 18^0$; $V_{dI} = 1$ (p.u.); $I_d = 0.5$ (p.u.)	5	$V_{11} = 0.9803\angle 10.737$; $V_{13} = 0.9597\angle 13.358$	$V_{dR} = 1.005$; $P_{dR} = 0.5025$; $a_R = 1.08$; $a_I = 1.15$; $Q_{dR} = 0.167$; $Q_{dI} = 0.2339$; $cos\phi_I = 0.9$; $cos\phi_R = 0.94$; NI = 6;
			6	$V_{11} = 0.9798\angle 11.1165$; $V_{13} = 0.9593\angle 11.7535$	$V_{dR} = 1.005$; $P_{dR} = 0.5025$; $a_R = 1.08$; $a_I = 1.15$; $Q_{dR} = 0.1698$; $Q_{dI} = 0.2339$; $cos\phi_I = 0.9058$; $cos\phi_R = 0.9474$; NI = 6;
			7	$V_{11} = 0.9797\angle 11.117$; $V_{13} = 0.9593\angle 11.7539$	$V_{dR} = 1.005$; $P_{dR} = 0.5025$; $a_R = 1.08$; $a_I = 1.15$; $Q_{dR} = 0.173$; $Q_{dI} = 0.2339$; $cos\phi_I = 0.9058$; $cos\phi_R = 0.9455$; NI = 6;
			8	$V_{11} = 0.9797\angle 11.1175$; $V_{13} = 0.9592\angle 11.7543$	$V_{dR} = 1.005$; $P_{dR} = 0.5025$; $a_R = 1.09$; $a_I = 1.15$; $Q_{dR} = 0.1768$; $Q_{dI} = 0.2339$; $cos\phi_I = 0.9058$; $cos\phi_R = 0.9433$; NI = 6;
			9	$V_{11} = 0.9796\angle 11.1181$; $V_{13} = 0.9592\angle 11.7548$	$V_{dR} = 1.005$; $P_{dR} = 0.5025$; $a_R = 1.09$; $a_I = 1.15$; $Q_{dR} = 0.1809$; $Q_{dI} = 0.2339$; $cos\phi_I = 0.9058$; $cos\phi_R = 0.9409$; NI = 6;
			10	$V_{11} = 0.9796\angle 11.1188$; $V_{13} = 0.9591\angle 11.7553$	$V_{dR} = 1.005$; $P_{dR} = 0.5025$; $a_R = 1.09$; $a_I = 1.15$; $Q_{dR} = 0.1855$; $Q_{dI} = 0.2339$; $cos\phi_I = 0.9058$; $cos\phi_R = 0.9381$; NI = 6;
			11	$V_{11} = 0.9795\angle 11.1195$; $V_{13} = 0.9591\angle 11.7559$	$V_{dR} = 1.005$; $P_{dR} = 0.5025$; $a_R = 1.1$; $a_I = 1.15$; $Q_{dR} = 0.1904$; $Q_{dI} = 0.2339$; $cos\phi_I = 0.9058$; $cos\phi_R = 0.9351$; NI = 6;
			12	$V_{11} = 0.9794\angle 11.1202$; $V_{13} = 0.959\angle 11.765$	$V_{dR} = 1.005$; $P_{dR} = 0.5025$; $a_R = 1.01$; $a_I = 1.15$; $Q_{dR} = 0.1958$; $Q_{dI} = 0.2339$; $cos\phi_I = 0.9058$; $cos\phi_R = 0.9318$; NI = 6;
			13	$V_{11} = 0.9794\angle 11.121$; $V_{13} = 0.959\angle 11.7571$	$V_{dR} = 1.005$; $P_{dR} = 0.5025$; $a_R = 1.1$; $a_I = 1.15$; $Q_{dR} = 0.2014$; $Q_{dI} = 0.2339$; $cos\phi_I = 0.9058$; $cos\phi_R = 0.9282$; NI = 6;
			14	$V_{11} = 0.9793\angle 11.1218$; $V_{13} = 0.9591\angle 11.755$	$V_{dR} = 1.005$; $P_{dR} = 0.5025$; $a_R = 1.11$; $a_I = 1.15$; $Q_{dR} = 0.2075$; $Q_{dI} = 0.2339$; $cos\phi_I = 0.9058$; $cos\phi_R = 0.9243$; NI = 6;
			15	$V_{11} = 0.9792\angle 11.1227$; $V_{13} = 0.9589\angle 11.7585$	$V_{dR} = 1.005$; $P_{dR} = 0.5025$; $a_R = 1.12$; $a_I = 1.15$; $Q_{dR} = 0.2138$; $Q_{dI} = 0.2339$; $cos\phi_I = 0.9058$; $cos\phi_R = 0.9201$; NI = 6;

$$\Delta P_i = P_i^{sp} - \sum_{k=1}^{n} V_i V_k Y_{ik} \cos(\theta_i - \theta_k - \phi_{ik}) - P_{dR} \quad (10)$$

$$\Delta Q_i = Q_i^{sp} - \sum_{k=1}^{n} V_i V_k Y_{ik} \sin(\theta_i - \theta_k - \phi_{ik}) - Q_{dR} \quad (11)$$

$$\Delta P_j = P_j^{sp} - \sum_{k=1}^{n} V_j V_k Y_{jk} \cos(\theta_j - \theta_k - \phi_{jk}) + P_{dI} \quad (12)$$

$$\Delta Q_j = Q_j^{sp} - \sum_{k=1}^{n} V_j V_k Y_{jk} \sin\left(\theta_j - \theta_k - \phi_{jk}\right) - Q_{dI} \quad (13)$$

where $P_{dR} = V_{dR} I_d, Q_{dR} = P_{dR} tan\phi_R, P_{dI} = V_{dI} I_d$, and $Q_{dI} = P_{dI} tan\phi_I$.

In the above equations, the equivalent active power injections 'P_{dR}' and 'P_{dI}' are usually specified or can be very easily computed by manipulation of the specified variables. However, for the equivalent reactive power injections Q_{dR} and Q_{dI}, the case is different, depending on the control strategy adopted for the DC link. For control strategies 1, 3, 4 and 5, ϕ_R and ϕ_I (and hence Q_{dR} and Q_{dI}) can be computed by manipulation of the specified variables. However, for control strategies 2 and 6, ϕ_R and ϕ_I (and hence Q_{dR} and Q_{dI}) are dependent on both the specified variables as well as the AC state variables, which are updated every iteration. This affects the convergence pattern. The steps involved in the computation of the active and reactive power injections pertaining to control strategies 1 and 2 only are detailed in Table B.1 of Appendix B. From Table B.1, it is observed that unlike control strategy-1, the reactive power injection in control strategy-2 is updated every iteration, adversely affecting the convergence. Although the steps involved in the computation of the power

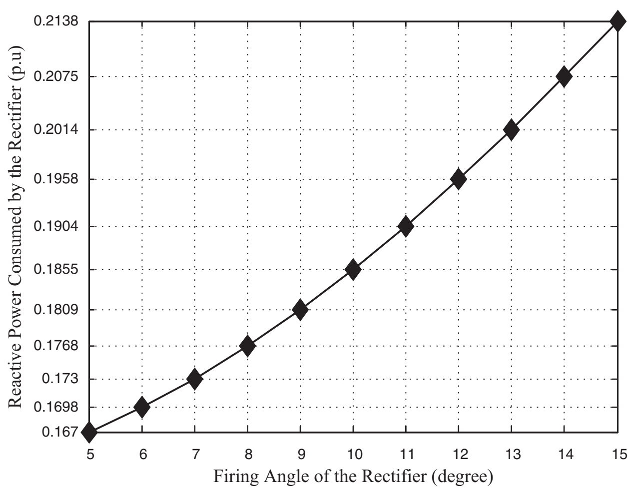

Figure 8 Variation of reactive power consumed by the rectifier with its firing angle.

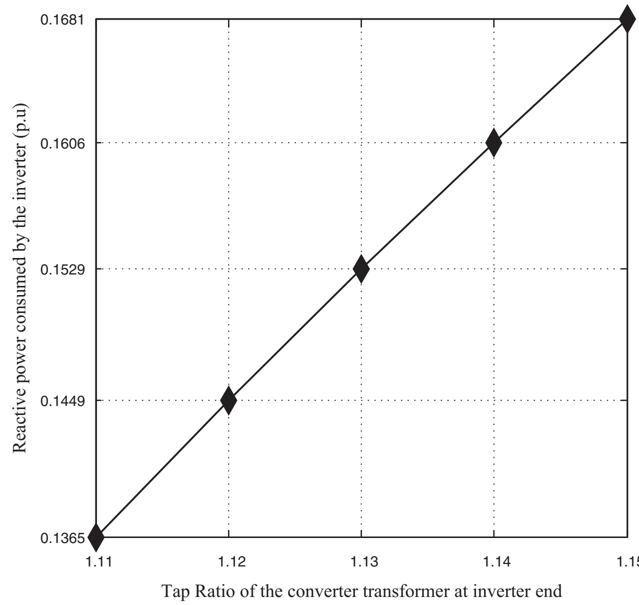

Figure 9 Variation of the reactive power consumed by the inverter with its tap setting.

Table 5 Variation of extinction angle and reactive power consumption of inverter with its transformer tap setting.

HVDC links		HVDC link specification		Power flow solutions	
Rectifier bus	Inverter buses	Control strategy-5	a_I	AC terminal buses	HVDC variables
11	13	$\alpha_R = 6^0$; $V_{dR} = 1$ (p.u.); $I_d = 0.35$ (p.u.)	1.11	$V_{11} = 0.9817\angle 10.8211$; $V_{13} = 0.964\angle 10.7882$	$V_{dI} = 0.9965$; $P_{dR} = 0.35$; $a_R = 1.1$; $Q_{dR} = 0.1408$; $Q_{dI} = 0.1365$; $\gamma_I = 15.4291^0$; $cos\phi_I = 0.9313$; $cos\phi_R = 0.9277$; NI = 11;
			1.12	$V_{11} = 0.9816\angle 10.8215$; $V_{13} = 0.9635\angle 10.7972$	$V_{dI} = 0.9965$; $P_{dR} = 0.35$; $a_R = 1.1$; $Q_{dR} = 0.1408$; $Q_{dI} = 0.1783$; $\gamma_I = 17.0756^0$; $cos\phi_I = 0.9235$; $cos\phi_R = 0.9277$; NI = 11;
			1.13	$V_{11} = 0.9816\angle 10.8218$; $V_{13} = 0.9629\angle 10.8058$	$V_{dI} = 0.9965$; $P_{dR} = 0.35$; $a_R = 1.0982$; $Q_{dR} = 0.1408$; $Q_{dI} = 0.1529$; $\gamma_I = 18.5595^0$; $cos\phi_I = 0.9158$; $cos\phi_R = 0.9277$; NI = 11;
			1.14	$V_{11} = 0.9815\angle 10.822$; $V_{13} = 0.9624\angle 10.8141$	$V_{dI} = 0.9965$; $P_{dR} = 0.35$; $a_R = 1.0983$; $Q_{dR} = 0.1408$; $Q_{dI} = 0.1606$; $\gamma_I = 19.9168^0$; $cos\phi_I = 0.9083$; $cos\phi_R = 0.9277$; NI = 11;
			1.15	$V_{11} = 0.9814\angle 10.8223$; $V_{13} = 0.9619\angle 10.822$	$V_{dI} = 0.9965$; $P_{dR} = 0.35$; $a_R = 1.1$; $Q_{dR} = 0.1408$; $Q_{dI} = 0.1681$; $\gamma_I = 21.172^0$; $cos\phi_I = 0.9009$; $cos\phi_R = 0.9277$; NI = 11;

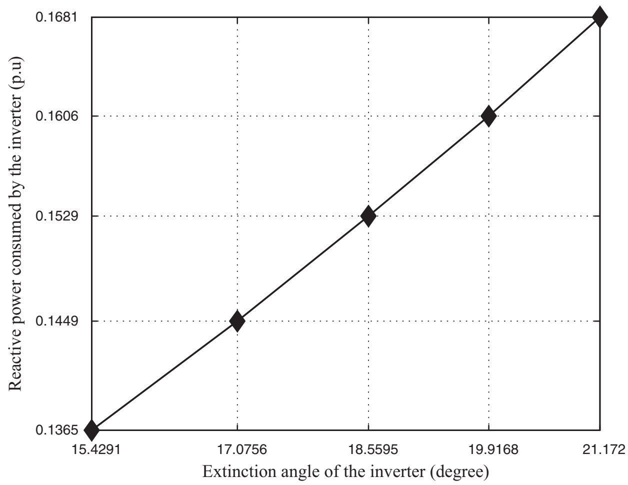

Figure 10 Variation of the reactive power consumed by the inverter with its extinction angle.

injections pertaining to control strategies 3, 4, 5 and 6 are not shown due to limitation of space, they can be done in a similar manner.

It is important to note the conventions of the signs of the equivalent real and reactive power injections representing the DC link. It is assumed that the rectifier consumes both real and reactive power from the AC grid while the inverter supplies real power and consumes reactive power from it.

5. Case studies and results

To analyze how AC–DC power flow convergence is affected by the control strategy adopted for the HVDC link, several case studies were carried out with multiple HVDC links incorporated in the IEEE 118-bus and IEEE 300-bus test systems [16]. All the simulations were carried out in MATLAB. Although several control strategies are feasible, due to a shortage of space, only case studies pertaining to seven typical control strategies are reported in this paper. Two comprehensive case studies on the IEEE 118-bus test system and three on the IEEE 300-bus test systems are reported. Each comprehensive case study comprises seven separate power flow studies, each pertaining to the application of a particular control strategy to a DC link. For all the case studies, the commutating reactance and the DC link resistance were chosen as 0.1 p.u. and 0.01 p.u. respectively. The number of bridges 'n_b' for all the converters [11] was taken to be equal to 2. To minimize the reactive power requirement at the rectifier and inverter terminals and the overall system losses, the values of the rectifier firing angles and the inverter extinction angles are kept within 5–7° and 15–22° respectively, for all the case studies. In a similar manner, the tap ratios of the converter transformers are set to keep the above control angles within the above limits. A convergence tolerance of 10^{-12} p.u. was uniformly adopted for all the case studies. In each of the case studies, 'NI' refers to the number of iterations taken by the algorithm to converge to the specified tolerance (10^{-12} p.u.). In general, 'NI' is representative of the degree of convergence of a power flow study.

5.1. Case I: First study of IEEE-118 bus system

In this study, a single HVDC link is incorporated in the transmission line between buses 11 and 13. The base case (without any HVDC link) active power flow in this line is found to be 40.81 MW. Subsequently, applying Control Strategy 1 to the HVDC link, its active power-flow is set to a value of 50 MW. The rectifier firing angle and the inverter extinction angle were set to 5° and 18° respectively. On account of the relationship between the inverter side DC voltage, the AC bus voltage magnitude, the converter transformer tap ratio and the power factor at the inverter end {Eq. (4)}, the inverter side DC voltage is set to a value of 1.0 p.u. These are detailed in columns 1–5 of Table 3. The power-flow solution corresponding to these specifications are also shown in columns 6–9 of Table 3. The state variables pertaining to the AC and DC systems are denoted as ACSV and DCSV respectively. It requires six iterations to converge. In a similar manner, the HVDC link specifications corresponding to the six other control strategies and their power-flow solution are shown in Table 3.

From Table 3, it is observed that almost similar convergence pattern is exhibited for all the control strategies except Control Strategy 2, 6 and 7 where the number of iterations taken to converge is more. This is reiterated from the convergence characteristics shown in Figs. 3–6, corresponding to the base case (without any HVDC link) and three typical control strategies 1, 2 and 6, respectively. In Figs. 3–6, 'error' refers to the maximum absolute power mismatch (in p.u.). From Figs. 3–6, it is observed that the power flow convergence with control strategy 1 is almost similar to that of the base case as the power injections (at the terminal buses connected to the rectifier and the inverter) can be computed apriori and remain constant. It is also observed from Figs. 3–6 that the convergence characteristics with control strategies 2 and 6 are adversely affected as compared to that with control strategy 1. This is due to the fact that with control strategies 2 and 6, the equivalent reactive power injections are updated in every iteration, as already explained in Appendix B. The convergence patterns for control strategies 3–5 and control strategy 7 although similar to control strategy 1 and control strategy 2 or 6 respectively, are not shown due to limitations of space.

The bus voltage profile for the power-flow solution pertaining to the case with control strategy 2 is shown in Fig. 7. It is observed that bus voltage profile hardly changes except the AC terminal buses connected to the rectifier and the inverter. However, the bus voltage profiles of the other case studies of Table 3 are not shown due to limitations of space.

It may be noted from Table 3 that for control strategy 3, the firing angle of the rectifier and the extinction angle of the inverter are maintained at constant values of 5° and 18°, respectively. This is done in order to minimize the reactive power consumptions of the converters. A separate case study was carried out to elaborate this. The rectifier firing angle was gradually increased from 5° to 15° while maintaining the DC current and voltage at the inverter end at 0.5 p.u. and 1 p.u., respectively. The specified quantities and the power flow solutions are shown in columns 3–4 and 5–6 of Table 4 respectively. The variation of the reactive power consumed by the rectifier with the firing angle is shown in Fig. 8. It is observed that the reactive power consumed by the rectifier 'Q_{dR}' increases

Table 6 Second study of IEEE 118-bus system.

HVDC link		P_{base} (pu)	HVDC link specification		Power flow solution			
From bus no	To bus no		Spec. values		ACSV		DCSV	
			Control strategy 1		AC terminal buses		HVDC variables	
6	7	0.3386	P_{dR} (pu)	0.5	V_6	0.99	V_{dR}	1.005
							I_d	0.4975
			V_{dI} (pu)	1.0	θ_6	11.037°	a_R	1.07
							a_I	1.12
			α_R (deg.)	5°	V_7	0.9878	$cos\phi_R$	0.94
							$cos\phi_I$	0.90
			γ_I (deg.)	18°	θ_7	11.150°	NI	6
			Control strategy 2		AC terminal buses		HVDC variables	
			P_{dR} (pu)	0.5	V_6	1.0	V_{dR}	1.005
							I_d	0.4975
			V_{dI} (pu)	1	θ_6	10.926°	α_R	12.419°
							γ_I	17.929°
			a_R	1.08	V_7	0.994	$cos\phi_R$	0.93
							$cos\phi_I$	0.90
			a_I	1.1	θ_7	11.079°	NI	8
			Control strategy 3		AC terminal buses		HVDC variables	
			I_d (pu)	0.5	V_6	0.99	V_{dR}	1.005
							P_{dR}	0.5025
			V_{dI} (pu)	1	θ_6	11.035°	a_R	1.07
							a_I	1.11
			α_R (deg.)	5°	V_7	0.9878	$cos\phi_R$	0.94
							$cos\phi_I$	0.90
			γ_I (deg.)	18°	θ_7	11.151°	NI	6
			Control strategy 4		AC terminal buses		HVDC variables	
			P_{dR} (pu)	0.5	V_6	1.00	V_{dR}	1.005
							I_d	0.4975
			V_{dI} (pu)	1	θ_6	10.92°	a_R	1.06
							γ_I	12.862°
			α_R (deg.)	5	V_7	0.997	$cos\phi_R$	0.94
							$cos\phi_I$	0.92
			a_I	1.08	θ_7	11.038°	NI	6
			Control strategy 5		AC terminal buses		HVDC variables	
			P_{dR} (pu)	0.5	V_6	0.99	V_{dR}	1.005
							I_d	0.4975
			V_{dI} (pu)	1	θ_6	11.036°	α_R	12.200°
							a_I	1.11
			a_R	1.09	V_7	0.9908	$cos\phi_R$	0.93
							$cos\phi_I$	0.90
			γ_I (deg.)	18°	θ_7	11.109°	NI	6
			Control strategy 6		AC terminal buses		HVDC variables	
			P_{dR} (pu)	0.5	V_6	1.00	V_{dR}	0.9946
							I_d	0.5027
			a_R	1.05	θ_6	10.92°	V_{dI}	0.9896
							α_R	5.6583°
			a_I	1.1	V_7	0.994	$cos\phi_R$	0.94
							$cos\phi_I$	0.90
			γ_I (deg.)	18°	θ_7	11.079°	NI	6
			Control strategy 7		AC terminal buses		HVDC variables	
			V_{dR} (p.u.)	1	V_6	1	V_{dI}	0.995
							γ_I	17.1234°
			I_d (p.u.)	0.5	θ_6	10.8952°	a_R	1.09
							P_{dR}	0.5
			a_I	1.1	V_7	0.9941	$cos\phi_R$	0.9144
							$cos\phi_I$	0.9099
			α_R (deg.)	6°	θ_7	11.0473°	NI	8

Table 7 First study of IEEE 300-bus system.

HVDC link		P_{base} (pu)	HVDC link specification		Power flow solution			
From bus no	To bus no		Spec. values		ACSV		DCSV	
			Control strategy 1		AC terminal buses		HVDC variables	
270	292	0.3652	P_{dR} (pu)	0.4	V_{270}	1.008	V_{dR}	1.004
							I_d	0.3984
			V_{dI} (pu)	1.0	θ_{270}	−11.41°	a_R	1.05
							a_I	1.09
			α_R (deg.)	5°	V_{292}	1.00	$cos\phi_R$	0.95
							$cos\phi_I$	0.91
			γ_I (deg.)	18°	θ_{292}	−10.69°	NI	7
			Control strategy 2		AC terminal buses		HVDC variables	
			P_{dR} (pu)	0.4	V_{270}	1.0005	V_{dR}	1.004
							I_d	0.3984
			V_{dI} (pu)	1	θ_{270}	−11.41°	α_R	10.174°
							γ_I	15.673°
			a_R	1.06	V_{292}	1.00	$cos\phi_R$	0.94
							$cos\phi_I$	0.92
			a_I	1.08	θ_{292}	−10.68°	NI	10
			Control strategy 3		AC terminal buses		HVDC variables	
			I_d (pu)	0.4	V_{270}	1.008	V_{dR}	1.004
							P_{dR}	0.4016
			V_{dI} (pu)	1	θ_{270}	−11.41°	a_R	1.09
							a_I	1.00
			α_R (deg.)	5°	V_{292}	1.00	$cos\phi_R$	0.95
							$cos\phi_I$	0.91
			γ_I (deg.)	18°	θ_{292}	−10.65°	NI	7
			Control strategy 4		AC terminal buses		HVDC variables	
			P_{dR} (pu)	0.4	V_{270}	1.008	V_{dR}	1.004
							I_d	0.3984
			V_{dI} (pu)	1	θ_{270}	−11.41°	a_R	1.05
							γ_I	19.036°
			α_R (deg.)	5	V_{292}	1.00	$cos\phi_R$	0.95
							$cos\phi_I$	0.90
			a_I	1.1	θ_{292}	−10.69°	NI	7
			Control strategy 5		AC terminal buses		HVDC variables	
			P_{dR} (pu)	0.4	V_{270}	1.0031	V_{dR}	1.004
							I_d	0.3984
			V_{dI} (pu)	1	θ_{270}	−11.42°	α_R	7.6894°
							a_I	1.09
			a_R	1.05	V_{292}	1.00	$cos\phi_R$	0.95
							$cos\phi_I$	0.91
			γ_I (deg.)	18°	θ_{292}	−10.69°	NI	7
			Control strategy 6		AC terminal buses		HVDC variables	
			P_{dR} (pu)	0.4	V_{270}	1.002	V_{dR}	1.0105
							I_d	0.3958
			a_R	1.08	θ_{270}	−11.41°	V_{dI}	1.0066
							α_R	13.551°
			a_I	1.1	V_{292}	1.00	$cos\phi_R$	0.93
							$cos\phi_I$	0.91
			γ_I (deg.)	18°	θ_{292}	−10.68°	NI	10
			Control strategy 7		AC terminal buses		HVDC variables	
			V_{dR} (p.u.)	1	V_{270}	0.99	V_{dI}	0.996
							γ_I	18.110^0
			I_d (p.u.)	0.4	θ_{270}	18.582°	a_R	1.08
							P_{dR}	0.4
			a_I	1.09	V_{292}	1	$cos\phi_R$	0.9232
							$cos\phi_I$	0.9138
			α_R (deg.)	6°	θ_{292}	19.310^0	NI	8

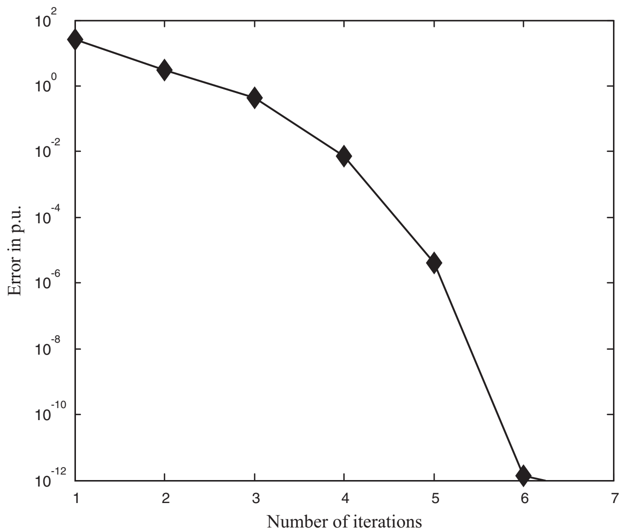

Figure 11 Convergence characteristics of base case power flow in IEEE-300 bus test system.

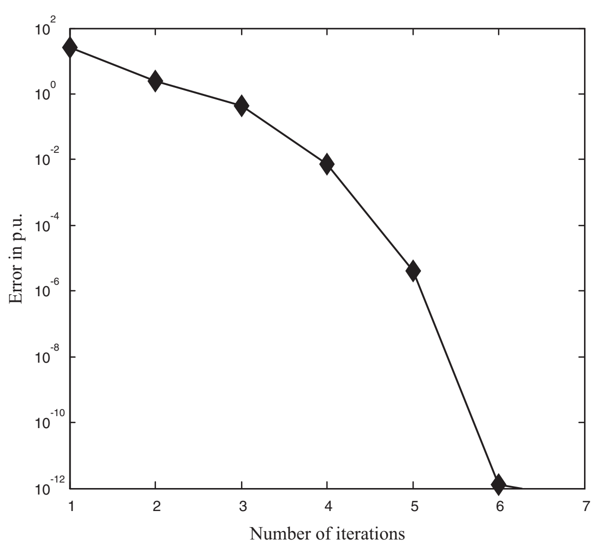

Figure 12 Convergence characteristics for the case study of Table 5 with control strategy 1.

as the firing angle of the rectifier 'α_R' increased. The tap setting of the rectifier transformer is kept within its specified limits to minimize the reactive power consumed by the rectifier.

In a similar manner, corresponding to control strategy 7 in Table 3, the tap setting of the inverter transformer is gradually increased from 1.11 to 1.15 while maintaining the DC voltage of the rectifier and the DC current to 1 p.u. and 0.35 p.u., respectively. The firing angle of the rectifier is also maintained to a constant value 6°. The specified quantities and the power flow solutions are shown in columns 3–4 and 5–6 of Table 5 respectively. The variation of the reactive power consumed by the inverter with the transformer tap ratio and extinction angle of the inverter is shown in Figs. 9 and 10 respectively. It is observed that the reactive power consumed by the inverter 'Q_{dI}' increases as the extinction angle of the inverter 'γ_I'

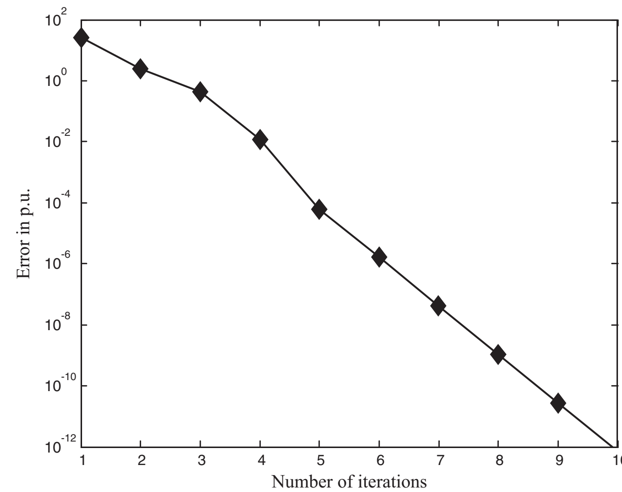

Figure 13 Convergence characteristics for the case study of Table 5 with control strategy 2.

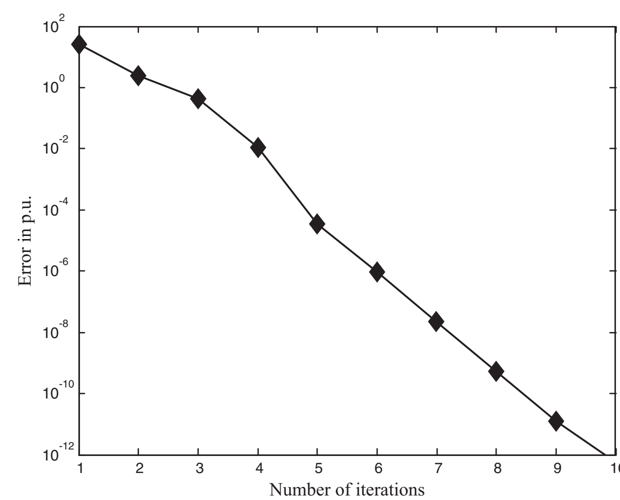

Figure 14 Convergence characteristics for the case study of Table 5 with control strategy 6.

increased. Therefore, the tap setting of the inverter is adjusted to minimize the extinction angle of the inverter and the reactive power consumed by the inverter.

5.2. Case II: Second study with the IEEE 118-bus system

In this study, a single HVDC link was incorporated in the transmission line between buses 6 and 7. The base case active power flow in this line was found to be 33.86 MW. Subsequently, applying Control Strategy 1 to the HVDC link, the active power flow is set to a value of 50 MW. The rectifier firing angle and the inverter extinction angle were again set to 5° and 18° respectively. The inverter side DC voltage is set to a value 1 p.u. These are detailed in columns 1–5 of Table 6. The power-flow solution corresponding to these specifications are also shown in columns 6–9 of Table 6. It requires six iterations to converge. In a similar manner, the HVDC link specifications corresponding to the five other control strategies and their

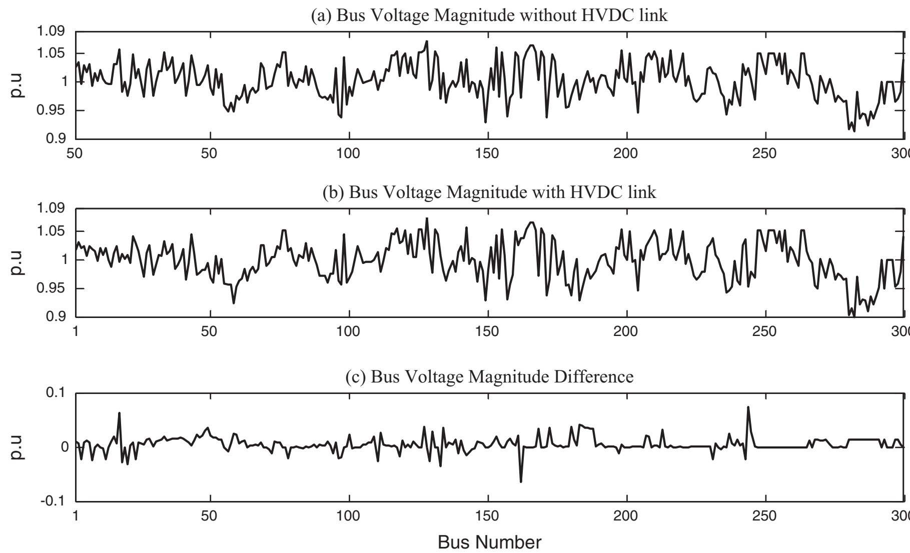

Figure 15 Bus voltage profile for the case study of Table 5 with control strategy 2.

power-flow solutions are shown in Table 6. It can be observed that NI is more for control strategy 2, as is expected. It is also observed that in Table 6, the convergence pattern corresponding to control strategies 2 and 6 are slightly better than those in Table 3. This is because the convergence pattern is also dependent on the location of the DC link i.e. the AC system buses between which the link is incorporated. This is reiterated from the subsequent case studies with the IEEE 300 bus system.

5.3. Case III: First study of IEEE 300-bus system

In this study, a HVDC link is first incorporated in the transmission line between buses 270 and 292. The base case power flow in this line is 36.52 MW. The power-flow with the HVDC link is set to 40 MW. For all the seven control strategies, the different HVDC link specifications along with the corresponding power-flow solutions are shown in Table 7.

From Tables 6 and 7, it can be observed that with the HVDC link incorporated, the IEEE 300-bus system takes more number of iterations to converge than the IEEE 118-bus system. Also, from Table 7, it is observed that similar convergence patterns is exhibited for all the control strategies except control strategies 2, 6 and 7, where the number of iterations taken to converge is more. This is reinforced from the convergence characteristics shown in Figs. 11–14, corresponding to the base case (without any HVDC link) and three typical control strategies 1, 2 and 6, respectively. From Fig. 11–14, it is observed that the power flow convergence with control strategy 1 is as good as that of the base case while those with control strategies 2 and 6 are adversely affected. This is expected, as the reactive power injections are updated every iteration with control strategies 2, 6 and 7 unlike in control strategy 1. The convergence characteristics for control strategies 3–5 and control strategy 7, although similar to control strategy 1 and control strategy 2 or 6, are not shown due to limitations of space.

The bus voltage profile for the power-flow solution pertaining to the case with control strategy 2 is shown in Fig. 15. It is observed that bus voltage profile hardly changes except the AC terminal buses connected to the rectifier and the inverter. However, due to lack of space, the bus voltage profiles of the other case studies of Table 7 could not be accommodated.

5.4. Case IV: Second study of IEEE 300-bus system

In this study, a HVDC link is first incorporated in the transmission line between buses 1 and 3. The base case power flow in this line is 24.04 MW. The power-flow with the HVDC link is set to 40 MW. For all the seven control strategies, the different HVDC link specifications along with the corresponding power-flow solutions are shown in Table 8.

From Table 8, it can be observed that almost identical convergence characteristics are exhibited for all the control strategies. In addition, for control strategy 2, 6 and 7, the number of iterations taken to converge is more, as expected. Also, in comparison with Table 7, the convergence pattern with control strategies 2, 6 and 7 are slightly better. This is because the convergence pattern also depends on the location of the DC link.

5.5. Case V: Third study of IEEE 300-bus system

In this study, a HVDC link is first incorporated in the transmission line between buses 199 and 197. The base case power flow in this line is 32.13 MW. The power-flow with the HVDC link is set to 40 MW. For all the seven control strategies, the different HVDC link specifications along with the corresponding power-flow solutions are shown in Table 9. From Table 9, it can be observed that the model exhibits almost similar convergence characteristics for all the control strategies except control strategies 2, 6 and 7. For control strategy 2, 6 and 7, the NI taken to converge is more, as is expected from the explanations given in Appendix B.

From the case studies, it is also observed that in addition to the control strategy adopted, the location of the DC link i.e. the system buses between which the DC link is incorporated, also affects the power flow convergence pattern, although to a lesser extent.

Table 8 Second study of IEEE 300-bus system.

HVDC link		P_{base} (pu)	HVDC link specification		Power flow solution			
From bus no	To bus no		Spec. values		ACSV		DCSV	
			Control strategy 1		AC terminal buses		HVDC variables	
3	1	0.2404	P_{dR} (pu)	0.4	V_3	1.0187	V_{dR}	1.004
							I_d	0.3984
			V_{dI} (pu)	1.0	θ_3	6.6208°	a_R	1.03
							a_I	1.08
			α_R (deg.)	5°	V_1	1.0147	$cos\phi_R$	0.95
							$cos\phi_I$	0.91
			γ_I (deg.)	18°	θ_1	6.4066°	NI	7
			Control strategy 2		AC terminal buses		HVDC variables	
			P_{dR} (pu)	0.4	V_3	1.0186	V_{dR}	1.004
							I_d	0.3984
			V_{dI} (pu)	1	θ_3	6.6218°	α_R	9.8257°
							γ_I	19.893°
			a_R	1.04	V_1	1.0145	$cos\phi_R$	0.94
							$cos\phi_I$	0.90
			a_I	1.09	θ_1	6.408°	NI	9
			Control strategy 3		AC terminal buses		HVDC variables	
			I_d (pu)	0.4	V_3	1.0187	V_{dR}	1.004
							P_{dR}	0.4016
			V_{dI} (pu)	1	θ_3	6.6206°	a_R	1.03
							a_I	1.08
			α_R (deg.)	5°	V_1	1.0147	$cos\phi_R$	0.95
							$cos\phi_I$	0.91
			γ_I (deg.)	18°	θ_1	6.4083°	NI	7
			Control strategy 4		AC terminal buses		HVDC variables	
			P_{dR} (pu)	0.4	V_3	1.017	V_{dR}	1.004
							I_d	0.3984
			V_{dI} (pu)	1	θ_3	6.641°	a_R	1.03
							γ_I	21.472°
			α_R (deg.)	5	V_1	1.0158	$cos\phi_R$	0.95
							$cos\phi_I$	0.89
			a_I	1.1	θ_1	6.4176°	NI	7
			Control strategy 5		AC terminal buses		HVDC variables	
			P_{dR} (pu)	0.4	V_3	1.0194	V_{dR}	1.004
							I_d	0.3984
			V_{dI} (pu)	1	θ_3	6.611°	α_R	6.2125°
							a_I	1.08
			a_R	1.03	V_1	1.0167	$cos\phi_R$	0.95
							$cos\phi_I$	0.91
			γ_I (deg.)	18°	θ_1	6.3904°	NI	7
			Control strategy 6		AC terminal buses		HVDC variables	
			P_{dR} (pu)	0.4	V_3	1.0186	V_{dR}	1.0264
							I_d	0.3897
			a_R	1.08	θ_3	6.6228°	V_{dI}	1.0225
							α_R	14.424°
			a_I	1.1	V_1	1.0146	$cos\phi_R$	0.93
							$cos\phi_I$	0.91
			γ_I (deg.)	18°	θ_1	6.4085°	NI	8
			Control strategy 7		AC terminal buses		HVDC variables	
			V_{dR} (p.u.)	1	V_3	1.0185	V_{dI}	0.996
							γ_I	17.3967°
			I_d (p.u.)	0.4	θ_3	36.623°	a_R	1.06
							P_{dR}	0.4
			a_I	1.07	V_1	1.0146	$cos\phi_R$	0.9232
							$cos\phi_I$	0.9172
			α_R (deg.)	6°	θ_1	36.4084°	NI	9

Table 9 Third study of IEEE 300-bus system.

HVDC link		P_{base} (pu)	HVDC link specification		Power flow solution			
From bus no	To bus no		Spec. values		ACSV		DCSV	
			Control strategy 1		AC terminal buses		HVDC variables	
199	197	0.3213	P_{dR} (pu)	0.4	V_{199}	1.008	V_{dR}	0.9044
							I_d	0.4423
			V_{dI} (pu)	0.9	θ_{199}	−22.19°	a_R	0.96
							a_I	1.00
			α_R (deg.)	10^{O}	V_{197}	1.0159	$cos\phi_R$	0.93
							$cos\phi_I$	0.88
			γ_I (deg.)	22°	θ_{197}	−22.63°	NI	7
			Control strategy 2		AC terminal buses		HVDC variables	
			P_{dR} (pu)	0.4	V_{199}	1.000	V_{dR}	0.9044
							I_d	0.4423
			V_{dI} (pu)	0.9	θ_{199}	−22.15°	α_R	8.819°
							γ_I	21.44°
			a_R	0.96	V_{197}	1.0124	$cos\phi_R$	0.94
							$cos\phi_I$	0.88
			a_I	1	θ_{197}	−22.64°	NI	9
			Control strategy 3		AC terminal buses		HVDC variables	
			I_d (pu)	0.4	V_{199}	1.000	V_{dR}	0.9040
							P_{dR}	0.3616
			V_{dI} (pu)	0.9	θ_{199}	−22.65°	a_R	0.95
							a_I	1.00
			α_R (deg.)	10°	V_{197}	1.0162	$cos\phi_R$	0.94
							$cos\phi_I$	0.88
			γ_I (deg.)	22°	θ_{197}	−22.65°	NI	7
			Control strategy 4		AC terminal buses		HVDC variables	
			P_{dR} (pu)	0.4	V_{199}	1.000	V_{dR}	0.9044
							I_d	0.4423
			V_{dI} (pu)	0.9	θ_{199}	−22.15°	a_R	0.96
							γ_I	21.625°
			α_R (deg.)	10^{0}	V_{197}	1.0157	$cos\phi_R$	0.93
							$cos\phi_I$	0.88
			a_I	1.0	θ_{197}	−22.15°	NI	7
			Control strategy 5		AC terminal buses		HVDC variables	
			P_{dR} (pu)	0.4	V_{199}	1.008	V_{dR}	0.9044
							I_d	0.4423
			V_{dI} (pu)	0.9	θ_{199}	−22.18°	α_R	7.839°
							a_I	0.9
			a_R	0.95	V_{197}	1.0193	$cos\phi_R$	0.94
							$cos\phi_I$	0.83
			γ_I (deg.)	22°	θ_{197}	−22.63°	NI	7
			Control strategy 6		AC terminal buses		HVDC variables	
			P_{dR} (pu)	0.4	V_{199}	1.000	V_{dR}	0.8985
							I_d	0.4452
			a_R	0.95	θ_{199}	−22.15°	V_{dI}	0.8941
							α_R	6.947°
			a_I	1	V_{197}	1.00123	$cos\phi_R$	0.94
							$cos\phi_I$	0.88
			γ_I (deg.)	22°	θ_{197}	−22.64°	NI	9
			Control strategy 7		AC terminal buses		HVDC variables	
			V_{dR} (p.u.)	1	V_{199}	1	V_{dI}	0.996
							γ_I	17°
			I_d (p.u.)	0.4	θ_{199}	7.8464°	a_R	1.08
							P_{dR}	0.4
			a_I	1.07	V_{197}	1.0129	$cos\phi_R$	0.9232
							$cos\phi_I$	0.9189
			α_R (deg.)	6°	θ_{197}	7.3457°	NI	10

Table A.1 Different base values for DC system.

$V_{dc\ base} = kV_{ac\ base}$; where $k = \frac{3\sqrt{2}}{\pi}n_b$
$I_{dc\ base} = \frac{\sqrt{3}}{k}I_{ac\ base}$
$Z_{dc\ base} = k^2 Z_{ac\ base}$
$R_{dc\ base} = \frac{3}{\pi}n_b X_{c\ base}$

6. Conclusions

For the power-flow solution of integrated AC–DC systems, the DC link control specifications bridge the gap between the number of independent equations and the number of unknown quantities. Depending on the application, several combinations of valid control specifications are possible. Each combination of a set of valid control specifications comprises a control strategy. It is observed that the power-flow convergence of integrated AC–DC systems is strongly affected by the control strategy adopted. For a majority of the possible control strategies, the equivalent real and reactive power injections at the concerned buses are independent of the NR iterative loop. However, for others, the equivalent reactive power injections need to be computed every NR iteration. This affects the convergence of the algorithm. This is validated by power flow convergence characteristics with different control strategies and multiple power flow case studies with application of seven different control strategies on DC links incorporated in the IEEE-118 and 300 bus test systems.

Acknowledgments

The authors are grateful to the Department of Electrical Engineering, Delhi Technological University, Delhi for the help and the support received. The authors are also indebted to Prof. Biswarup Das of the Department of Electrical Engineering, IIT Roorkee, for his suggestions on the implementation of AC–DC power flow.

Appendix A. See Table A.1.

$$V_{ac\ base} = V(line\ to\ line\ rms\ voltage)$$

$$I_{ac\ base} = \frac{S_{base}}{\sqrt{3}V_{ac\ base}} \quad \text{(A.1)}$$

$$Z_{ac\ base} = \frac{V_{ac\ base}}{\sqrt{3}I_{ac\ base}} \quad \text{(A.2)}$$

Appendix B. As already explained in Section 4, for solving the AC power flow, the equivalent active and reactive power injections at the AC terminal buses connected to the converters need to be computed. The steps involved in the computation of the active and reactive power injections for control strategies 1 and 2 is shown in Table B.1 below.

From Table B.1, it can be observed that the active power injections can be computed prior to the AC power flow. It is also observed that in Control Strategy-1, the quantities ϕ_R and ϕ_I and hence the reactive power injections Q_{dR} and Q_{dI} can be computed prior to the AC power flow by manipulation of the specified variables. On the other hand, in Control Strategy-2, they are also dependent on the AC power flow variables and thus, need to be updated every iteration.

Although the steps pertaining to the other control strategies could not be detailed due to a shortage of space, they can also be done in a similar manner.

References

[1] Arrillaga J, Watson NR. Computer modelling of electrical power systems. 2nd ed. John Wiley & Sons Ltd; 2003.
[2] Kundur P. Power system stability and control. Tata McGraw-Hill Publishing Co. Ltd.; 2007.
[3] Wang XF, Song YH. Malcolm irving. Modern Power Syst Anal 2008.
[4] Braunagel Duane A, Kraft Leonard A, Whysong Jewel L. Inclusion of DC converter and transmission equations directly in a Newton power flow. IEEE Trans Power Appar Syst 1976;PAS-95:76–87.
[5] Arrillaga J, Bodger PS. AC–DC load flows with realistic representation of the converter plant. Proc Inst Elect Eng 1978;125:41–6.

Table B.1 Steps to compute active and reactive power injections in control strategies 1 and 2.

Control Strategy-1		Control Strategy-2	
Specified quantities $\alpha_R, P_{dR}, \gamma_I, V_{dI}$	Unknown quantities $a_R, a_I, V_{dR}, \phi_R, \phi_I, I_d, P_{dI}$	Specified quantities a_R, P_{dR}, a_I, V_{dI}	Unknown quantities $\alpha_R, \gamma_I, V_{dR}, \phi_R, \phi_I, I_d, P_{dI}$
Step 1: Compute $V_{dR} = \frac{V_{dI}+\sqrt{V_{dI}^2+4R_{dc}P_{dR}}}{2}$		Step 1: Compute $V_{dR} = \frac{V_{dI}+\sqrt{V_{dI}^2+4R_{dc}P_{dR}}}{2}$	
Step 2: Compute $I_d = \frac{P_{dR}}{V_{dR}}$		Step 2: Compute $I_d = \frac{P_{dR}}{V_{dR}}$	
Step 3: Compute $P_{dI} = V_{dI}I_{dI}$		Step 3: Compute $P_{dI} = V_{dI}I_{dI}$	
Step 4: Compute $\cos\phi_R = \frac{V_{dR}cos\alpha_R}{V_{dR}+X_cI_d}$		Step 4: Compute $\cos\phi_R = \frac{V_{dR}}{a_RV_i}$; **Note 1:** V_i is an AC power flow variable and is updated every iteration. Hence, $\cos\phi_R$ changes in every iteration	
Step 5: Compute $Q_{dR} = P_{dR}tan\phi_R$		Step 5: Compute $Q_{dR} = P_{dR}tan\phi_R$	
Step 6: Compute $\cos\phi_I = \frac{V_{dI}cos\gamma_I}{V_{dI}+X_cI_d}$		Step 6: Compute $\cos\phi_I = \frac{V_{dI}}{a_IV_j}$; **Note 2:** V_j is also an AC power flow variable and is updated every iteration, along with $\cos\phi_I$	
Step 7: Compute $Q_{dI} = P_{dI}tan\phi_I$; **Note:** P_{dR} is specified. P_{dI}, Q_{dR} and Q_{dI} can be computed prior to the AC power flow and hence, are independent of the iterative loop		Step 7: Compute $Q_{dI} = P_{dI}tan\phi_I$; **Note 3:** P_{dR} is specified. P_{dI} can be computed prior to the AC power flow. However, Q_{dR} and Q_{dI} depend upon ϕ_R and ϕ_I respectively, and need to be updated every iteration	

[6] El-Marsafawy MM, M Mathur R. A new, fast technique for load flow solution of integrated multi terminal DC/AC systems. IEEE Trans Power Appar Syst 1980;PAS-99:246–55.
[7] Arrillaga J, Harker BJ, S Turner K. Clarifying an ambiguity in recent AC–DC load flow formulations. IEE Proc C 1980;127:324–5.
[8] Smed T, Andersson G, Sheble GB, Grigsby LL. A new approach to AC/DC power flow. IEEE Trans Power Syst 1991;6(3):1238–44.
[9] Reeve J, Fahmy G, Stott B. Versatile load flow method for multi terminal HVDC systems. IEEE Trans Power Appar Syst 1977;PAS-96:925–33.
[10] Fudeh H, Ong CM. A simple and efficient AC–DC load flow method for multiterminal DC systems. IEEE Trans Power Appar Syst 1981;PAS-100(11):4389–96.
[11] El- Hawary ME, T Ibrahim S. A new approach to AC–DC load flow analysis. Electric Power Res 1995;33:193–200.
[12] Liu Chongru, Zhang Boming, Hou Yunhe, Wu Felix F, Liu Yingshang. An improved approach for AC–DC power flow calculation with multi Infeed DC systems. IEEE Trans Power Syst 2011;26(2):862–9.
[13] Liu Congru, Bose Anjan, Hou Yunhe. Discussion of the solvability of HVDC power flow with a sequential method. Electric Power Res 2012;92:155–61.
[14] Messalti Sabir, Belkhiat Saad, Saadate Shahrokh, Flieller Damien. A new approach for load flow analysis integrated AC–DC power systems using sequential modified Gauss Seidal methods. Eur Trans Electr Power 2012;22(4):421–32.
[15] Kilic Ulas, Ayan Kursat. Optimizing power flow of AC–DC power systems using artificial bee colony algorithms. Electr Power Energy Syst 2013;53:592–602.
[16] http://www.ee.washington.edu/research/pstca/.

Shagufta khan is currently pursuing the Ph.D. degree in electrical engineering at the Delhi Technological University, Delhi, India.

Suman Bhowmick is currently is an Associate Professor in electrical engineering at the Delhi Technological University, Delhi, India. His research interests include power systems and electrical machines.